

International Workshop on the  
Materials Imaging and Dynamics Instrument  
at the European XFEL

European Synchrotron Radiation Facility (ESRF), Grenoble, France

October 28-29, 2009

Report of Working Group II on  
*X-ray Photon Correlation Spectroscopy*

(June 2010)

Authors:

Gerhard Grübel, DESY, Hamburg (Germany)

Christian Schüssler-Langeheine, Universität zu Köln, Köln (Germany)

with contributions from:

Christian Gutt, DESY, Hamburg (Germany)

Peter Wochner, MPI-MF, Stuttgart (Germany)

Brian Stephenson, APS-ANL, Chicago (USA)

Bogdan Sepiol, University of Vienna, Wien (Austria)

Anders Madsen, ESRF, Grenoble (France)

Mikhail Yurkov, DESY, Hamburg (Germany)

# I Introduction

The first *International Workshop on the Materials Imaging and Dynamics Instrument at the European XFEL* was held at the European Synchrotron Radiation Facility (ESRF) in Grenoble, France on October 28-29, 2009. The scientific program started out with a general overview about the European XFEL project, followed by an introduction to the *Materials Imaging and Dynamics (MID) Instrument* that is supposed to address the needs of two communities: the coherent X-ray diffraction imaging community interested in materials science questions and the X-ray photon correlation spectroscopy (XPCS) community interested in time domain studies. The two fields were reviewed in tutorial introductory talks by C. Gutt (XPCS) and I. Vartanians (CXDI) in order to facilitate the discussions. The scientific cases were then re-iterated and complemented by three presentations on CXDI (S. Ravy, A. Beerlink and E. Vlieg) and on XPCS (P. Wochner, B. Stephenson and L. Cipelletti). A subsequent session on instrumentation covered X-ray optics and beam transport, and the status of area detector developments for CXDI and XPCS. This was complemented by reports on the related instruments that are being build at the Linac Coherent Light Source (LCLS) at SLAC.

On day 2 the audience split up into two parallel sessions and formed working groups to discuss specific technical and scientific aspects of the planned MID station. The working group topics were:

- *Coherent X-ray Diffraction Imaging (WG I)*  
co-chaired by O. Thomas and I. Vartanians
- *X-Ray Photon Correlation Spectroscopy (WG II)*  
co-chaired by C. Schüssler-Langeheine and G. Grübel

The program of Working Group II comprised three short presentations on i) Atomic diffusion investigations by XPCS (B. Sepiol), ii) Recent XPCS activities and their relation to XPCS experiments (A. Madsen) and iii) X-ray speckles and higher order correlations from liquids (H. Sinn). The discussion in the XPCS workgroup focused on:

- Detectors: pixel size, number of pixels, frame-rate, accessible q-range
- Source parameters: energy, pulse pattern, pulse length and polarization
- Beamline optics: monochromaticity, focusing, degree of coherence, diagnostics
- Sample environment: temperature, external fields, pump pulses

The present report summarizes results and conclusions of these discussions. The participants of this working group are listed in the Annex. Chapters III.4 and III.5 address the request to identify prototypical experiments and their eventual impact on the detector requirements. A compilation (by E.L. Saldin, E.A. Schneidmiller, and M.V. Yurkov) of the expected properties of the radiation generated by the SASE-1 undulator that will give light to the MID instrument is attached in Annex VII.5.

It has to be noted that this workshop took place only a few weeks after the start-up of the Linac Coherent Light Source (LCLS) at Stanford. Since similar instruments as the ones discussed here will be available at the LCLS the participants of this working group pointed out that specific instrumentation details might need to be reviewed and reconsidered in view of the experience gained at LCLS.

## II Scientific Motivation

The scientific motivation for XPCS at a Free Electron Laser Source has been defined in the technical Design Report (TDR) for the XFEL [1], iterated upon on several occasions [2] and stems from the possibility to access complex dynamics on the nanoscale. Complex nanoscale dynamics is an omnipresent phenomenon which is investigated at the frontier of condensed matter research. It comprises a multitude of phenomena such as visco—elasticity and dissipation in liquids, polymer dynamics, protein folding, crystalline phase transitions or the switching of domains. The time-scales of interest range from femtoseconds to seconds. The study of fast ( $t \ll 1 \mu\text{s}$ ) dynamics at large momentum transfers  $Q$  was restricted up to now to the energy domain (inelastic) techniques. This however will change with the new FEL sources providing extremely brilliant ( $B > 10^{33} \text{ ph/s/mm}^2/\text{mrad}^2/0.1\% \text{ bw}$ ) and highly coherent X-ray beams. For the first time one will be able to study fast dynamics in the time domain, thus giving direct access to the dynamic response function  $S(Q,t)$ , instead of  $S(Q,\omega)$ , which is of central importance for a variety of phenomena such as fast non-equilibrium dynamics initiated e.g. by a short pump pulse. The experimental program will comprise studies of:

### II.1 Coherence and Correlations

Excellent coherence properties are among the most prominent features of the novel X-ray Free-Electron Laser sources. A comprehensive understanding of the XFELs coherence and correlation properties is of profound fundamental interest but also a necessary condition for performing coherence based experiments like XPCS and XXDI. Simulations, that predict the mode structure and the degree of coherence of the self-amplified stimulated emission (SASE) radiation will be compared with the results. The expected high degree of coherence will open a route towards investigating intermittent, heterogeneous, and non-gaussian dynamics via higher order time correlation functions.

### II.2 Study of glassy dynamics

When rapidly cooled below their freezing points, most liquids form metastable glassy or amorphous phases. This applies for a wide variety of materials including organic liquids, metallic alloys, oxides such as silica, polymer materials, and many others.

XPCS measures the time constants of a system as a function of wave vector and gives a rich direct information about the dynamic properties through the shape of the correlation functions. Covering a wide region of  $Q$  and  $t$  is very important for understanding the nature of the dynamics in glassforming systems both on the atomic scale and on the nanoscale. It is proposed to undertake studies spanning a very large range of time scales ( $10^{-12}$  to  $10^3$  s) in order to observe the evolution of the dynamics from liquid to glassy behavior as the temperature or pressure is changed. In order to cover the very large range of time scales, different experimental set-ups will need to be applied.

### II.3 Surface XPCS with an XFEL

A fundamental issue for all liquids is the onset of non-classical behavior at short length scales (i.e. large momentum transfers) where the assumption of continuum hydrodynamics breaks down. This happens e.g. at the surface of complex fluids when the scattering arises from individual molecules within the scattering volume which in the case of capillary waves undergo circular motions exponentially damped into the liquid material. Thanks to the unprecedented coherent flux of the XFEL a huge range in  $Q$  and  $t$  can be

covered which is very important for the understanding of the nature of the dynamics on both the atomic and nanoscale. It is expected to have important impact on controversial topics such as a wavelength dependent surface tension [3] or surface viscosity [4].

## II.4 Time-resolved magnetic scattering

Free-electron laser (FEL) sources based on SASE radiation can provide intense and ultrashort (femtosecond) pulses from the vacuum ultraviolet (VUV) to the X-ray range. These sources have the potential to record a magnetic diffraction pattern from a sample within a few femtosecond exposure and thus to probe elementary magnetization dynamics such as spin-flip processes and their coupling to the electronic system on their intrinsic time scales in the femtosecond (fs) regime. At the same time nanometer spatial resolution and element-specific information is provided allowing to access the complex composition of technologically relevant magnetic media and devices.

Using soft X-ray SASE photons resonant magnetic diffraction from a  $[\text{Co}(1.2\text{nm})/\text{Pd}(0.7\text{nm})]_{50}$  multilayer sample in transmission geometry was recorded [5,6]. The data were taken at the Co  $L_3$  edge by using the 5<sup>th</sup> harmonic and integrating for 1000s or in a single shot at the Co  $M_{2,3}$  edge. In the multilayer samples of this composition magnetic domains with alternating up and down magnetization form with a typical spatial correlation length of the order of 200-300 nanometers. Depending on the experimental conditions the single shot data at the Co M edge could be taken without modifying the sample thus opening the door to XPCS type studies.

Optimized setups for soft X-ray wavelengths will lead to intensity gains of 2-3 orders of magnitude which will make optical pump and X-ray diffraction probe measurements possible by using a single FEL pulse. The high intensities delivered on ultrafast timescales in combination with the high degree of spatial coherence of the FEL radiation will allow in the future the measurement of element specific spatial correlation functions in magnetic systems.

Similar experiments to be carried out in the energy regime covered by the MID instrument comprise rare earth systems and their L-edges to be used in resonant magnetic scattering experiments

## II.5 Non-equilibrium dynamics

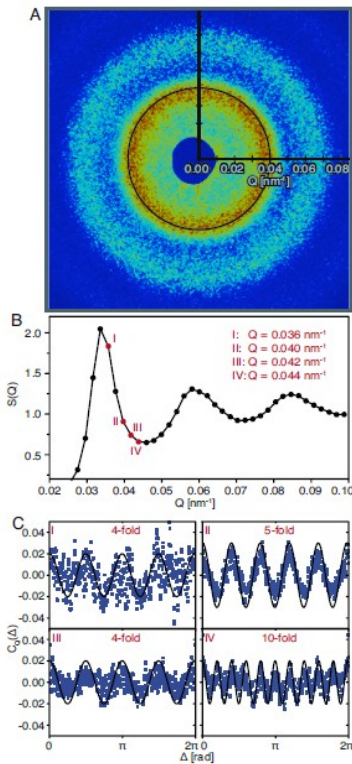
When a disordered homogeneous material is rapidly brought to a new set of conditions, corresponding e.g. to the coexistence of two equilibrium phases, a spatial pattern of domains of the two phases develops. A change of conditions can e.g. be accomplished by a rapid quench from a high temperature to a low one below the miscibility gap. The result of such a quench is the creation of a microstructure of interconnecting domains. These domains grow by coarsening in order to minimize the areas of the domain walls that separate the phases. While the time averaged behavior of such systems is reasonably well understood information on the statistics of fluctuations about this average behaviour (which differs from classical fluctuation statistics) is however scarce because conventional methods are not easily applicable since, by the nature of the process, absolute time matters. Only a time domain method, such as XPCS, can address such processes. Here fluctuations about the average intensity can be quantified by means of a two time ( $t_1$ ,  $t_2$ ) intensity correlation  $C(Q, t_1, t_2)$  function. XFEL will allow the study of the early (short time) stages of these processes. The XPCS pump-probe configuration will be ideally suited for any type, but in particular fast, non-equilibrium process. The pump or trigger source for reactions or transformations may comprise optical lasers, the XFEL, a Terahertz source, pulsed electric and magnetic fields and/or others.

At the workshop new fields, accessible to XPCS, were emerging. These comprise:

## II.6 X-ray Cross Correlation Analysis (XCCA) techniques for liquids

The interest in higher order correlation techniques stems from the fact that systems that do not exhibit translational symmetry in turn might be able to accommodate different local symmetries in the same system, such as icosahedral order. Such local symmetries might also be of transient nature and exist only for short times. The access to local properties is typically prevented by the intrinsic spatial (and temporal) averaging mechanisms inevitably occurring in conventional diffraction experiments with (partially coherent) light. In a recent prototype study a simple quasi-static hard-sphere glass system was investigated with partially coherent X-rays from a storage ring source [7]. A simple 4-point cross-correlation function  $C_Q(\Delta)$  was applied, where  $\varphi$  refers to the azimuthal angle of scattering into an annulus with reciprocal radius  $Q = |\mathbf{Q}|$ :

$$C_Q(\Delta) = (\langle I(Q, \varphi) I(Q, \varphi + \Delta) \rangle_\varphi - \langle I(Q, \varphi) \rangle_\varphi^2) / \langle I(Q, \varphi) \rangle_\varphi^2$$



The analyzed data reveal an unexpected 5-fold oscillation of the correlation function indicative of an up to now hidden 5-fold symmetry of locally ordered structures in the studied hard-sphere glass (Figure 1). It was shown furthermore that bond-orientational order symmetries slowly relax as a function of time at a given  $Q$  value. This result opens a new door to the investigation of e.g. (atomic scale) metallic glasses [8] or magnetically correlated systems. The access to transient local symmetries and locally ordered structures is of prime interest for our understanding of molecular fluids, in particular water. For this cross-correlation technique it is essential, that the number of illuminated particles in the sample volume is relatively small, in the order of  $10^7$ - $10^8$ .

Figure 1:

Experimental data and XCCA results. (A) CCD image showing a typical intensity spectrum with speckle structure. (B) Angular averaged structure factor of the image in A, which is the standard radial intensity distribution. (C) Experimental results after applying the cross-correlator  $C_Q(\Delta)$  to the data in A at different  $Q$  values. Solid lines are guide to the eyes.

## II.7 Atomic diffusion by XPCS

XPCS is a method capable of determining atomic dynamics, in particular the elementary diffusion step, in arbitrary systems, i.e. not restricted to certain favoured elements or isotopes, and over a wide dynamic range from nanoseconds to hours [9]. As XPCS is presently limited by the available coherent X-ray intensity, XPCS at the XFEL is a promising candidate to fill this gap.

One could imagine to carry out XPCS measurements using the diffuse scattering arising from disordered single crystalline and from amorphous alloys. Measuring the correlation time as a function of the scattering vector will give an unambiguous microscopic picture of the mechanism of atomic diffusion. For conventional XPCS, where one correlates frames taken a certain time interval apart, the accessible

timescales are limited only by the length of the experiment on the one side and the speed of the detector on the other side. For still faster dynamics the split-pulse technique (c.f. III.1.2) can be used.

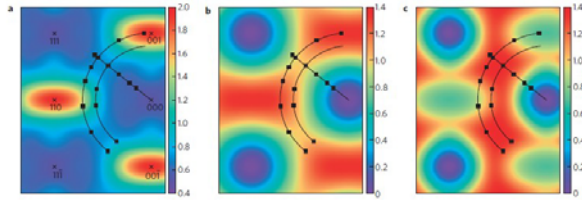


Figure 3 | Visualization of equation (4) for nearest-neighbour exchanges in the (110) plane in reciprocal space. The values for the short-range order intensities are taken from ref. 8. The black squares are positions of measurement projected onto the plane. The outer arc corresponds to Fig. 4a, the inner arc to Fig. 4b and the straight line to Fig. 4c. a. The static scattered intensity  $I_{S0}(\mathbf{q})$ , that is, the numerator of equation (4). b. The incoherent linewidth  $1 - \sum_{\mathbf{n}} n \cos(\mathbf{s} \cdot \mathbf{q})$ , that is, the denominator of equation (4). c. The coherent linewidth  $(1 - \sum_{\mathbf{n}} n \cos(\mathbf{s} \cdot \mathbf{q})) / I_{S0}$ , that is, the inverse of  $r(\mathbf{q})$ .

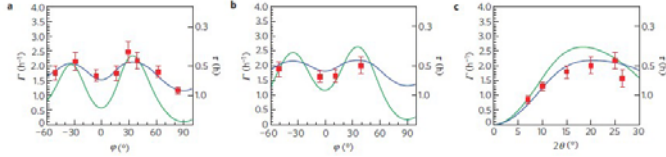


Figure 2: Visualization for nearest-neighbour exchanges in the (110) plane in reciprocal space and experimental correlation times together with fits for three one-dimensional scans through reciprocal space (from ref. 9)

## II.8 Dynamical heterogeneities in soft matter

Dynamical heterogeneities have been observed in a variety of soft matter systems although mostly accompanying slow dynamics. This is due to the lack of appropriate sources and detectors. It has been shown that such fluctuations in the dynamic behavior can be conveniently characterized by “Time Resolved Correlation Analysis” [10]. The variance of the degree of correlation vs. age is calculated which necessitates the use of a 2d detector. The variance (denoted dynamical susceptibility) is a four-point correlator in the intensity and closely related to the  $\chi_4$  factor characterizing the degree of spatial heterogeneity in glasses. An overview of the field and non-exponential correlation functions is given in Ref. 11.

## III The XPCS technique

### III.1 XPCS modes

X-ray Photon Correlation Spectroscopy (XPCS) probes the dynamic properties of matter by analyzing the temporal correlations between photons scattered by the sample. Correlations of the scattered intensity can be quantified via the normalized time correlation function  $g(\tau) = \langle n(t)n(t+\tau) \rangle / \langle n \rangle^2$ , where  $n(t)$  is the number of detected photons at time  $t$  and the brackets denote the time average. XPCS requires the sample to be illuminated coherently and the scattering pattern from a disordered sample is actually a speckle pattern. The accessible time window(s) will naturally be influenced by the specific time structure of the XFEL. To exploit the unique features of the XFEL three types of XPCS techniques have been proposed:

- i) Sequential or movie mode
- ii) Delay-line mode
- iii) Pump-probe mode

In “sequential” or “movie-mode” the normalized time correlation function  $g(\tau) = \langle n(t)n(t+\tau) \rangle / \langle n \rangle^2$  yields

$$g(\tau) = 1 + A(Q) |f(Q,\tau)|^2 \quad (3.1)$$

and thus access to the desired intermediate scattering function  $f(Q,\tau)$ . Here,  $A$  is a measure of the contrast or visibility. In delay-line mode one measures  $S(\tau) = I(t) + I(t+\tau)$ , where  $I$  is the measured intensity, and thus the access to  $f(Q,\tau)$  is given via:

$$c_2(\tau) = ( \langle S(\tau)^2 \rangle - \langle S(\tau) \rangle^2 ) / \langle S(\tau) \rangle^2 = 1/2 (1 + |f(Q,\tau)|^2) \quad (3.2)$$

The angular size  $S$  of an individual speckle is given by

$$S = (\lambda/W) * L \quad (3.3)$$

where  $\lambda$  is the wavelength,  $L$  the distance sample-detector and  $W$  is beam defining dimension (collimating aperture, sample size). The contrast or visibility  $A(Q)$  is given by

$$A(Q) = \sqrt{\langle I^2 \rangle - \langle I \rangle^2} / \langle I \rangle \quad (3.4)$$

If the spatial resolution of the detector (with pixel size  $P$ ) does not allow to resolve individual speckle one will observe a reduced contrast which is given by:

$$A_{\text{eff}} = A (1/[1+(P/S)^2]) \quad (3.5)$$

and for  $n$  photon pulses the signal-to-noise (SNR) ratio is given by:

$$\text{SNR} \sim A(Q) n / [1+(P/S)^2] * I \quad (3.6)$$

### III.1.1 The “sequential” or “movie-mode” technique:

The high time-averaged coherent X-ray flux from the XFEL, averaged over the 0.1 s repetition rate, can allow one to investigate slow (longer than  $10^{-1}$  s) dynamics collecting a sequence of speckle patterns on an area detector and using analysis techniques similar to the ones applied today.

The specific time structure of the XFEL will also allow to take dynamic data within the 600  $\mu\text{s}$  long macro-bunches. The shortest time will here be given by the micro-bunch separation of 200 ns<sup>1</sup>. It might turn out to be favorable to divide up this time window in logarithmic time bins thus requiring a 2-D detector to operate at 5 MHz frame rate but only with a limited number of frames to be stored. The “movie-mode” technique is illustrated in Figure 3.

<sup>1</sup>) recently changed to 220 ns.

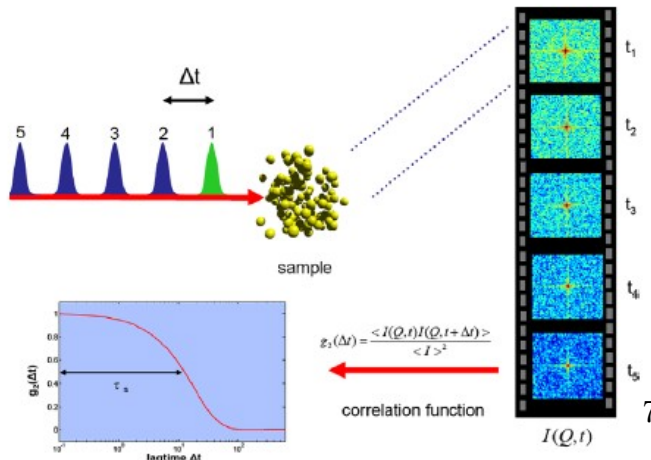


Figure 3: Illustration of the XPCS sequential or “movie-mode” technique.

### III.1.2 Split-pulse technique:

The concept of the split-pulse technique is to split each x-ray pulse into two equal-intensity pulses separated in time, but propagating along the same path. The scattering from the two pulses will then be collected during the same exposure of an area detector. If the sample is static on the time scale of the two pulses, then the contrast in the summed speckle pattern will be the same as that from a single pulse. If, on the other hand, the sample evolves on this time scale, then the summed speckle pattern will have lower contrast. Thus by analyzing a set of such patterns, each for a different time delay, the correlation times of the system can be measured, on time scales down to the minimum pulse duration. A pulse splitter with a path length difference variable from  $3 \times 10^{-4}$  to 3 m would give delay times from about  $10^{-12}$  to  $10^{-8}$  seconds.

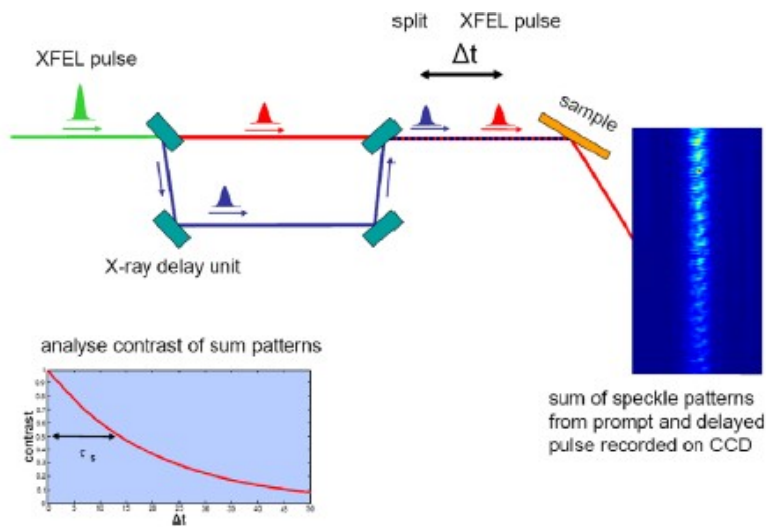


Figure 4 :  
Illustration of the XPCS split-pulse technique

### III.1.3 Pump-probe technique:

The XPCS pump-probe technique (Fig. 5) compares two speckle pattern: one before exposing the sample to a pump pulse and one taken a time interval  $\Delta t$  after the pump pulse. The pump sources triggering reactions and transformations may comprise optical lasers, the XFEL itself (X-ray pump X-ray probe), a Terahertz source, pulsed electric and magnetic fields, shock waves, and/or others. This allows to address time scales between 100 fs and typically 200 ns or longer.

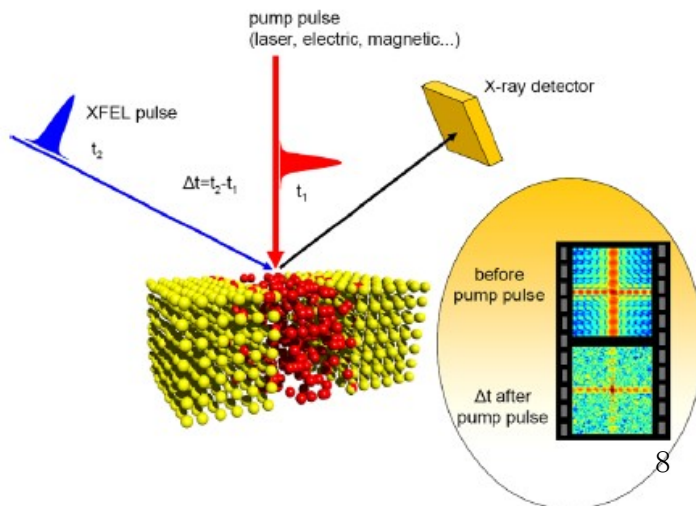


Figure 5:  
Illustration of the XPCS pump-probe technique

### III.2 Temperature and damage issues

For dynamics studies, one would like to avoid heating the sample by more than a few degrees during the measurement. In the following we consider adiabatic heating by each pulse, over time scales too small for significant heat flow, so that the temperature rise is determined by the heat capacity of the material. The amount of sample heating in the adiabatic case can be evaluated using an analysis developed for the LCLS case [2]. Fig. 6 shows a comparison of the quantities  $N_{\text{MIN}}$  (the minimum required number of photons per pulse to give sufficient signal per speckle),  $N_{\text{MAX}}$  (the maximum tolerable photons per pulse to avoid sample disturbance) and  $N_{\text{AVAIL}}$  (the available photons per pulse). These are plotted as a function of sample composition for two energies, using  $\Delta T_{\text{MAX}} = 1$  K, for a beam focussed to  $10 \mu\text{m}$  diameter, and two types of samples, having relatively narrow ( $M_{\text{corr}}=1000$ ; nanoscale cluster) or broader scattering ( $M_{\text{corr}}=10$ ; liquid or glass). The calculation predicts that XPCS will be feasible when the value of  $N_{\text{MIN}}$  is lower than both  $N_{\text{MAX}}$  and  $N_{\text{AVAIL}}$  (shaded areas). The result depends strongly on sample composition and photon energy.

Figure 6 indicates that XPCS experiments are feasible in the adiabatic limit for low Z materials. This would e.g. apply for single crystalline Al ( $Z=13$ ;  $M_{\text{corr}} = 1000$ ) while being a borderline case if in the molten state. Furthermore, single crystalline ( $M_{\text{corr}} = 1000$ ) materials seem to benefit from higher X-ray energies. However, because of the order-of magnitude uncertainty in several quantities, these calculations do not provide exact limits, but do indicate that feasibility will depend upon photon energy, sample composition and scattering power.

Some experimental data on damage issues encountered with magnetic CoPt multilayers in the soft x-ray regime ( $E = 0.8$  keV) has been reported recently [6].

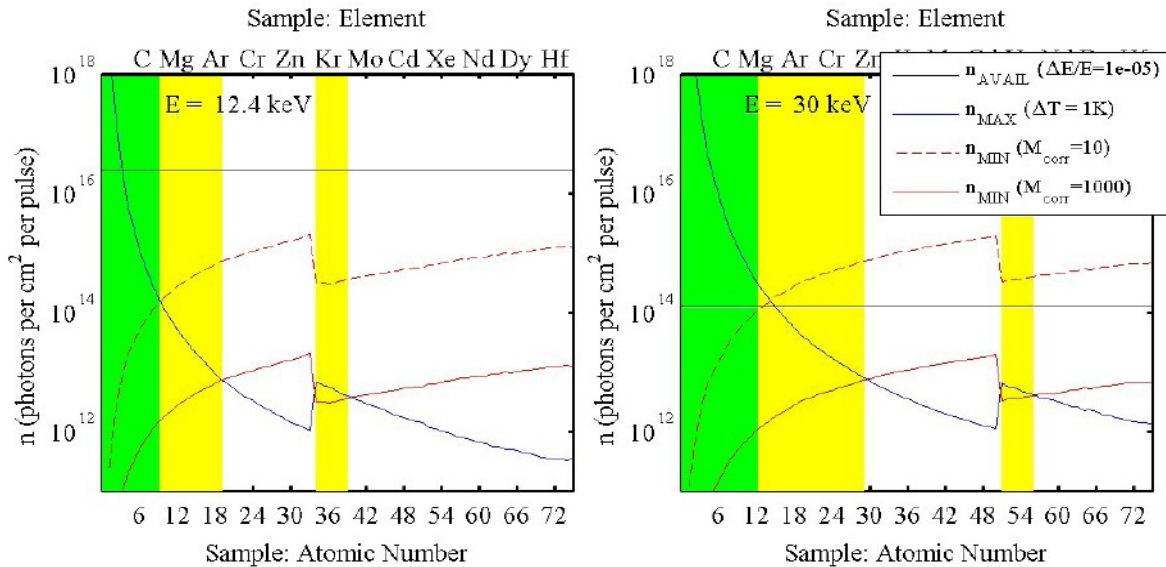


Figure 6: Comparison of the calculated number of photons per pulse for a  $10\mu\text{m}$  diameter beam from XFEL ( $N_{\text{AVAIL}}$ ), that is commensurate with a 1K heating ( $N_{\text{MAX}}$ ), and that is required for XPCS for two types of samples, a typical liquid or glass ( $M_{\text{corr}}=10$ ) or a nanoscale cluster ( $M_{\text{corr}}=1000$ ). Experiments are feasible in the shaded areas: green for experiments with with broad scattering (e.g. liquids), yellow for experiments with narrow scattering patterns.

### III.3 Intensity estimates

The temperature and damage estimates in paragraph III.2 indicate the feasibility of XPCS experiments in the adiabatic limit for low Z materials. In the following the temperature rise of the sample and the signal rates are estimated for XCCA type and dynamics experiments on i) molecular fluids, e.g. water and ii) glasses, such as  $B_2O_3$  or  $NiZr_2$ .

Figure 7 and Figure 8 show incident flux, absorption lengths, photons/atom/pulse, adiabatic temperature rise, counts/speckle/pulse, and the counts/speckle/pulse/1K temperature rise.

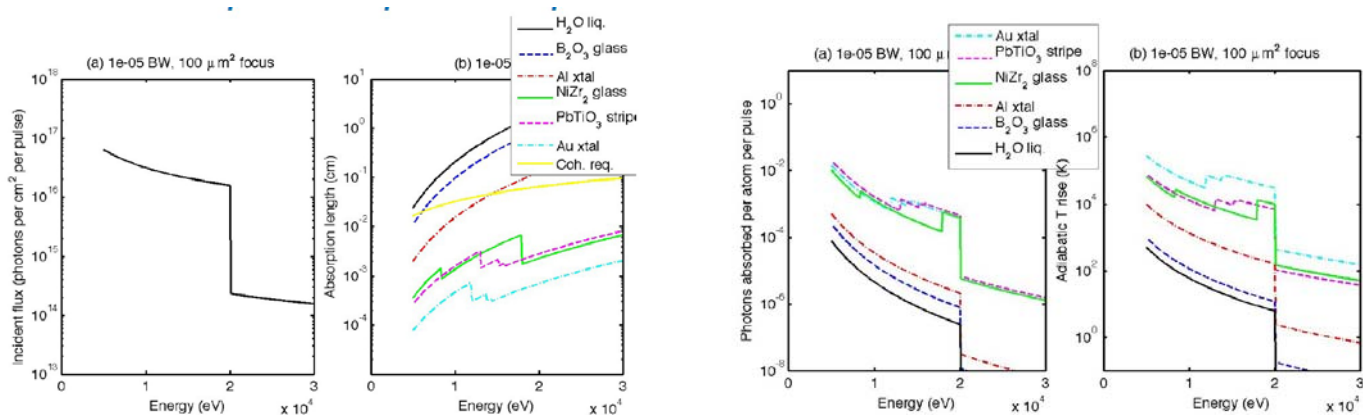


Figure 7: Incident flux, absorption lengths, photons/atom/pulse and adiabatic temperature rise.

Figure 7 (right) shows an adiabatic temperature rise of less than 100 K for water at 12 keV. The T rise for  $B_2O_3$  seems also moderate while all the other materials seem not to be feasible using the fundamental and the given parameters. The signal rates are indicated in Figure 8. For water one expects a countrate of about 0.1 ct/pulse/speckle compatible with XCCA analysis. The glasses are a bit more favourable. For XPCS type studies, limiting the T rise to 1 K one obtains signal rates of order 0.001 for water, quite similar to the glassy systems.

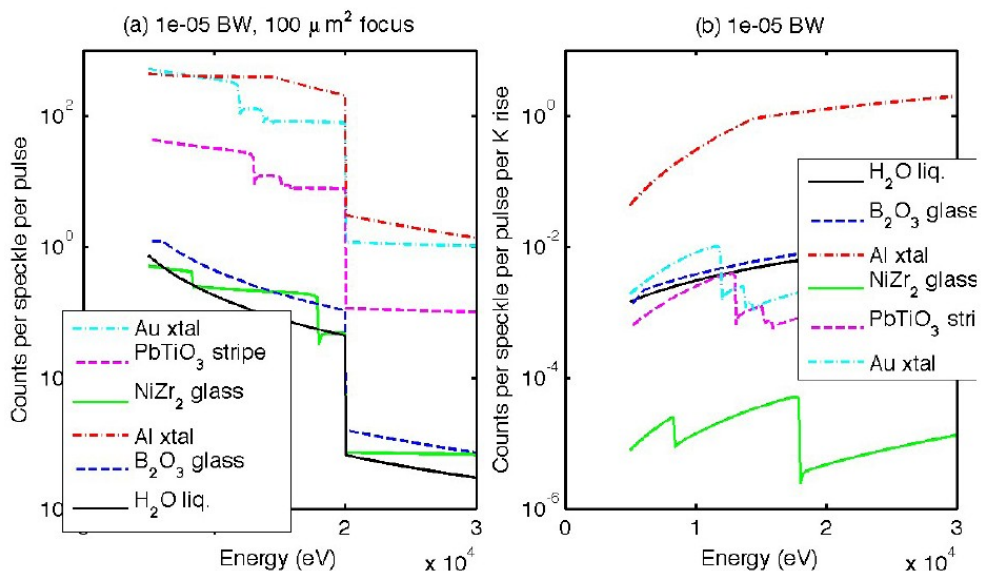


Figure 8: Counts/speckle/pulse, and the counts/speckle/pulse/1K temperature rise.

### III.4 Prototypical Experiments

In this chapter we shall focus on the beam parameters of two prototypical (multiple exposure, non-destructive) XPCS applications, a small angle scattering (SAXS) experiment and a wide angle scattering (WAXS) experiment. XPCS requires that the changes in the sample introduced by the  $n$ -th X-ray pulse are negligible or at least small enough so that a comparison of the  $n$ -th speckle pattern with the subsequent pattern(s) is interpretable in terms of the usual time-correlation functions. This might e.g. imply that the temperature change during the data acquisition time is small. In order to achieve this, the illuminating coherent beam (of size  $W$ ) should be chosen as large as reasonably possible.

First we consider a prototypical SAXS experiment, namely the diffusion of small nano-particles in a solvent. Assuming a particle radius of 15 nm, a viscosity of 1 mPas (water at  $T=298$  K) we find correlation times between 1074  $\mu\text{s}$  at  $Q=0.9 \times 10^{-3} \text{ \AA}^{-1}$  and 400 ns at  $Q=4.0 \times 10^{-2} \text{ \AA}^{-1}$  as shown in Figure 9. This is a time window that can be covered in the XFEL movie mode since it coincides with the time regime of an XFEL macro-bunch ( $200 \text{ ns} < t < 600 \text{ micro seconds}$ ).

The scattering intensity is also shown in figure 9 for a  $100 \times 100 \mu\text{m}^2$  beam with  $10^{10}$  ph/pulse. The intensity is calculated for a single detector pixel of  $1 \mu\text{rad}$  size. For a “hard sphere” system we expect correlations to develop at  $Q$  of about  $0.02 \text{ \AA}^{-1}$ . The expected count rates in that  $Q$  regime will be a few counts/pulse. It should be noted that this example is a very favorable one due to the very high electron density contrast for the chosen silica/water system.

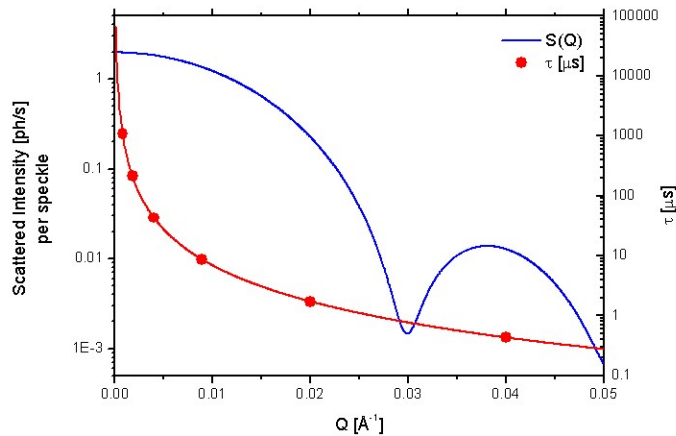


Figure 9: Scattering intensity [ph/pulse] (left) and correlation times [ $\mu\text{s}$ ] for a suspension of nanoparticles (see text).

We assume a temperature rise of  $\Delta T = Q/3Nk_B$  where  $Q$  is the energy absorbed from the photon beam in a volume determined by the absorption length of water (2.9 mm at  $1 \text{ \AA}$ ) and the size  $W \times W$  of the beam. For a  $155 \times 155$  microns beam of  $10^{10}$  ph/pulse ( $\Delta E/E = 10^{-5}$ ) we find  $\Delta T = 0.2$  K for water. If we were to require that the temperature may not rise by more than 1 K we may expose the sample to 5 consecutive shots per bunch train compatible with movie mode. Here we assume that the energy of the beam is fully converted into heat and any heat dissipation is ignored.

Second, we consider a WAXS experiment. There is a whole wealth of experiments involving length scales in the Angstrom regime thus implying momentum transfers of up to several inverse Angstroms. A prototypical example is water with a structure factor peak around  $2 \text{ \AA}^{-1}$ . We require that the temperature increase/pulse remains low enough so that the sample can support e.g. at least 2 pulses and does not warm up by more than 1 K. This is e.g. valid for a  $100 \times 100 \mu\text{m}^2$  beam carrying  $10^{10}$  ph/pulse.

### III.5 Detector Issues

The use of 2-D detectors will be mandatory for XPCS and XCCA experiments since scattering signals are expected to be weak and statistically relevant data will in many cases only be obtainable by using 2-D detectors. One important parameter for the 2-D detector(s) is the size of the detector pixel  $P$  since XPCS requires sensitivity to individual speckles. Ideally individual speckles with size  $S$  should be resolved allowing one to compute time-autocorrelation functions and only the correlation functions of equivalent speckles are allowed to be averaged. Thus

$$P \leq S = (\lambda/W) \times R \quad (3.7)$$

Here  $W$  denotes the beam size and  $R$  the distance between sample and detector. A frequently used working point is defined by requesting the pixel size to equal the beam size yielding

$$S = \text{sqrt}(\lambda R) \quad (3.8)$$

A first set of detector specifications was compiled for the Technical Design Report [1]. There an angular pixel size of 4  $\mu\text{rad}$  was specified ( $W=25 \mu\text{m}$ ) A sample-detector distance of 25m for low  $Q$  experiments and about 10m for large  $Q$  experiments would translate for the low  $Q$  (SAXS) experiments to pixel sizes of about 50  $\mu\text{m}$  (Eq. 3.8) to 100  $\mu\text{m}$  (Eq. 3.7). For large  $Q$  (WAXS) experiments the pixel size was estimated to about 50  $\mu\text{m}$  using Eq. 3.7. This set of parameters needs to be partly revisited in view of i) novel XPCS applications in particular in the WAXS regime and ii) further insight in the damage/heatload conditions to be encountered in the envisaged experiments.

In the following we shall focus on (multiple exposure, non-destructive) XPCS applications only and try to evaluate the impact of non-adapted pixel sizes on the outcome of an XPCS experiment for two experimental configurations:

I) Localized Scattering (fully covered by the detector)

This might apply to Small Angle Scattering (SAXS) in the forward direction or a situation where e.g. a single or few well defined diffraction peaks are to be measured.

II) Extended scattering (larger than the detector area)

This might be the case e.g. for large angle scattering (WAXS) of a molecular liquid spanning a full annulus at large momentum transfer  $Q$  with the scattering in addition being wide in the radial direction.

Common aspects to be considered are:

- i) XPCS experiments require the sample to be illuminated coherently, requiring that the maximum path length difference between two rays may not exceed the longitudinal coherence length  $\xi_l = \lambda / (\Delta\lambda/\lambda)$  in order to avoid a loss in contrast. This is usually not crucial in SAXS experiments since the  $Q$  values are small but might become a very serious issue in WAXS geometry. The longitudinal coherence length can be increased by reducing the energy bandwidth  $\Delta\lambda/\lambda$  of the beam (via monochromatization) at the expense of (coherent) flux.

- ii) In SAXS geometry the full length of the experimental hall might be available ( $R \approx 40\text{m}$ ). This is not the case in a large angle WAXS geometry.

### III.5.1 Localized SAXS scattering experiment

We consider in the following a prototypical SAXS experiment, namely the diffusion of small nanoparticles in a solvent. The scattering is assumed to be smaller than the considered detector area.

As shown in Annex VII.2 the signal to noise ratio in this geometry is given by

$$R_{sn} \sim (I_0 \Delta\theta P) A/R = (I_0 \Delta\theta P) / [R (1+P^2/S^2)] \quad (3.9)$$

where  $A=1/(1+P^2/S^2)$  is a measure of the contrast,  $I_0$  is the incident flux,  $\Delta\theta$  denotes the angular width of the scattering signal,  $L$  the distance sample to detector and  $P, S$  the pixel and speckle sizes, respectively.  $R_{sn}$  peaks for  $P=S$  and  $R_{sn} \sim I_0/W$ . This tells us that smaller beam sizes are preferable for a given  $I_0$ . However for smaller and smaller beam sizes sample heating beyond an acceptable value will set in and  $I_0$  needs to be reduced leading to smaller  $R_{sn}$  values. This happens for the given example at a beam size  $W = 155 \mu\text{m}$  (if  $\Delta T < 0.2\text{K}$  is required) and is illustrated in Figure 10 for two different detector pixel sizes ( $P1: 200 \mu\text{m}$  and  $P2: \mu\text{m} 50$ ). As can be seen from Figure 10 the  $R_{sn}$  values start to decrease when the minimum “tolerable” beamsize is reached. As can be seen from the figure the best  $R_{sn}$  achievable with a mismatched ( $200 \mu\text{m}$ ) pixel is (in arbitrary units) about 7.5 while with a  $50 \mu\text{m}$  pixel a  $R_{sn} = 25$  can be achieved. The  $R_{sn}$  loss in this example is thus a factor of about 3.3. (Note that the  $50$  micron pixel size is actually already slightly too big for a  $155$  micron beam).

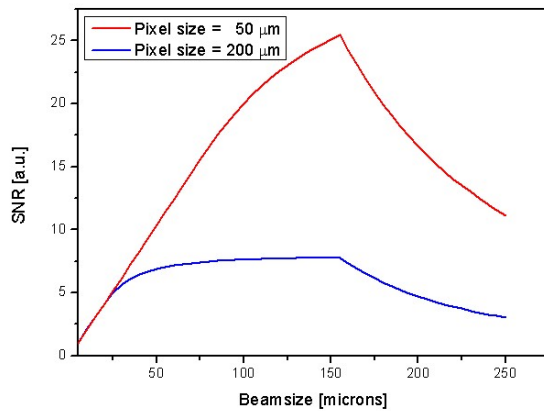


Figure 10:  
Signal-to-noise ratio  $R_{sn}$  for XPCS measurement with detectors of two different pixel sizes. ( $I_0 (W=50\mu\text{m}) = 1$ )

Inspection of Eq. (3.9) reveals that SAXS experiments carried out with a 2-D detector with mismatched pixel size (here  $200 \mu\text{m}$  vs.  $50 \mu\text{m}$ ) and an available sample to detector distance of  $40$  meters lead to  $R_{sn}$  losses smaller than a factor of about  $3.3$  in the given example. Compensation for the  $R_{sn}$  loss would require longer data acquisition times that scale quadratically with  $R_{sn}$  and would thus require (for the given example) a  $10$  times longer data acquisition time. This might be acceptable for very strongly scattering samples but might rapidly become a problem for weakly scattering specimens and/or systems more vulnerable to heatload.

It has been proposed to remedy the effects of a mismatched pixel by putting a (small) aperture in

front of a detector pixel element. As shown in Annex VII.3 for the SAXS configuration the signal to noise ratio  $R^{M_{sn}}$  in this case is given by

$$R^{M_{sn}} \sim (I_o \Delta\theta P_m^2) / [RP (1+P_m^2/S^2)] \quad (3.10)$$

where  $P_m$  is the size of the (masked pixel). As shown in Annex VII.3 masking in forward direction does not remedy the problem since the increase in speckle contrast is penalized by the decrease in intensity per pixel and thus  $R^{M_{sn}} < R_{sn}$ .

Although details may vary from experiment to experiment we would conclude that angular pixel sizes between  $1 \mu\text{rad}$  and  $\leq 4 \mu\text{rad}$  are necessary for SAXS experiments.

### III.5.2 WAXS experiments

We consider in the following a prototypical WAXS experiment, e.g. water with a structure factor peak around  $2 \text{ \AA}^{-1}$ . The scattering is distributed over  $2\pi$  and larger than the considered detector. As shown in chapter III.4 we require that the temperature increase/pulse remains low enough so that the sample can support at least 2 pulses and does not warm up by more than 1 K. This is still valid for a  $100 \times 100 \mu\text{m}^2$  beam carrying  $10^{10}$  ph/pulse and we use these parameters for the following example.

As described before and quantified in [Eq. 31, Abernathy et al., J. Synchrotron Rad., 5, 37 (1998)] the contrast  $A$  of a speckle depends upon the bandpath  $\Delta\lambda/\lambda$ , geometrical quantities such as the sample-width and sample thickness and upon the momentum transfer  $Q$ . This is illustrated for an example in Fig. 11.

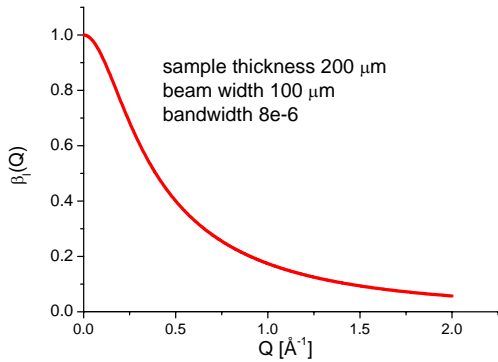


Figure 11: Contrast  $A = \beta(Q)$  as a function of momentum transfer.

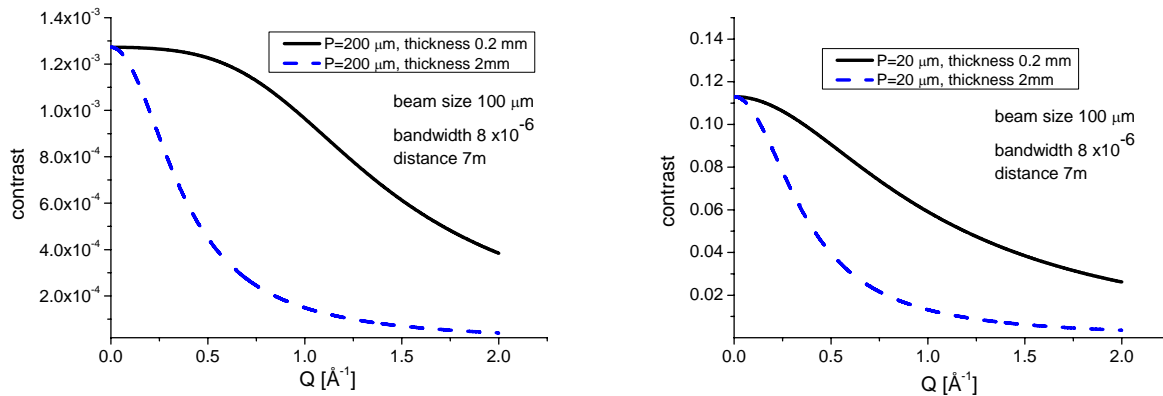


Figure 12: Contrast as a function of momentum transfer for two different pixel sizes and two different sample thicknesses.

Applying Eq.'s 3.7 and 3.8 we find that the necessary pixel sizes now are 7  $\mu\text{m}$  or 26  $\mu\text{m}$  respectively for  $R=7\text{m}$  (scattering angle  $2\theta \approx 20$  deg.). We will assume in the following a 20  $\mu\text{m}$  pixel as being an appropriate choice. Under this assumption we have evaluated the speckle contrast for a 20  $\mu\text{m}$  pixel detector and a 200  $\mu\text{m}$  detector for 2 different samples thicknesses: 0.2 mm and 2mm. The results are shown in Fig. 12. For  $Q = 1 \text{ \AA}^{-1}$  we observe a contrast of about 0.06 for a 0.2 mm sample and a 20  $\mu\text{m}$  pixel. For the 200  $\mu\text{m}$  pixel a contrast of about  $9 \times 10^{-4}$  is expected.

As noted before the scattering is larger than the detector of size  $D \times D$ . The intensity per pixel is given by  $I=I_0 \times P^2/R^2$ . Thus the number of pixels  $N=(D/P)^2$  and

$$R_{\text{sn}} \sim D I_0 A(Q) P / R^2 \quad (3.11)$$

We thus expect that the signal-to-noise ratio between the matched to mismatched pixel is about 10. Compensation for the  $R_{\text{sn}}$  loss would require longer data acquisition times that scale quadratically with  $R_{\text{sn}}$  and would require (for the given example) a 100 times longer data acquisition time. Given the fact that the expected count rates in these experiments are of order 0.1 to 0.001 per pixel one is led to conclude that these types of experiments will become unfeasible without a detector with adapted pixel size and/or insufficient number of pixels.

Note that the adapted detector would ideally have to cover the complete  $2\pi$  scattering annulus at the respective wavevector. The consequences of limited  $2\pi$  coverage are presently studied in detail and will be appended when available. In zeroth order it can be predicted that a reduction of the angular coverage by a factor of  $1/N$  results in a loss of contrast by  $(1/N)^2$ , i.e. a coverage of  $\pi/2$  results in a loss of contrast of  $1/16$ . Furthermore, a limited coverage also impedes the analysis of anisotropic scattering patterns severely, which is e.g. the case for partially aligned anisotropic colloidal particles or anisotropically strained or textured metallic glasses.

Masking in the given example does not lead to any advantage. One can however not exclude that there might be situations (involving intermediate pixel sizes and scattering areas) that might benefit from the masking approach.

### III.5.3 Detector Specification

As worked out in chapters III.5.1 and III.5.2 area detectors with adapted pixel sizes are crucial for XPCS experiments. These sizes are  $\leq 4 \mu\text{rad}$  for the SAXS configuration and 2-3  $\mu\text{rad}$  for the WAXS configuration. It is also apparent that the expected countrates are low thus permitting detector architectures with a very limited counter depth. We note that the discussed examples assumed that only few frames were to be recorded per bunchtrain. This very assumption depends on a further (experimental) verification of the heatload response, on the choice of the very sample and the details of the experiment. If e.g. very fast dynamics is to be measured with the help of a X-ray delay line one will have to face a throughput of about 1% thus reducing the heatload by about a factor of 100. This could e.g. be used towards a higher framerate configuration.

Based on the preceding discussion we are led to the following summary of (updated) detector specifications as given in table 1:

Table 1:

|                           |   | Detector I (SAXS) | Detector II (WAXS)        |
|---------------------------|---|-------------------|---------------------------|
| Single photon resolution: | yes (poisson limited)                                   | x                 | x                         |
| Photon energy range [keV] | 6 – 15  | x                 | x                         |
| Quantum efficiency        | > 0.8   | x                 | x                         |
| Environment               | ambient   | x                 | x                         |
| Harmonics discrimination  | no  | x                 | x                         |
| Pixel Size $\mu$ rad      |   | $\leq 4$          | 2 - 3                     |
| Number of Pixels          |   | 1k x 1k (2k x2 k) | 1k x 1k (10e8 on annulus) |
| Signal rate/pixel/bunch   |   | few up to 1000    | few up to 100             |
| Vacuum compatibility      | no  | x                 | x                         |
| Preprocessing             | option (hit finding algorithm, autocorrelator,...)      |                   |                           |
| Timing                    | timing optimized (5 MHz frame-rate, log time bins, ...) |                   |                           |

## IV Requirements

The technical requirements to carry out XPCS experiments at the European XFEL have been discussed in terms of source parameters, specifications for beamline and detector and for the sample environment. The technical requirements for XPCS at the MID station are:

### Photon energy

XPCS experiments will mostly be carried out using the undulator fundamental. Some XPCS experiments may use higher photon energies by going to higher undulator harmonics or by opening the undulator gap. No experiments above 36 keV are presently envisioned ( $E > 15$  keV not considered in the detector specifications yet). Certain experiments require photon energies below 12 keV down to 6 keV in order to suppress fluorescence background. In this lower energy range the photon energy could be fixed during one experiment such that a change on a week to week (experiment to experiment) time scale could be sufficient. Default operation at  $1.5\text{\AA}$  would provide some flexibility in the requirements for the necessary 2-D detectors.

### Pulse pattern

The possible time scale that can be covered by a split and delay line is practically limited to a few ns. With a pulse spacing of 200 ns this leaves a range of time scales on which dynamics cannot be studied. An option to reduce the pulse spacing between at least certain bunches in the bunch train, e.g., by delay generation in the gun would allow to bridge this gap and be consequently very helpful. The development of an adapted delay line [12] should be pursued. Since many XPCS experiment will be luminosity limited, an increase of the repetition rate of the bunch trains to 20 or 30 Hz would be of interest.

### Pulse length

A reduction of the pulse length from 100 fs to shorter times can be expected to reduce the radiation damage of the sample and is therefore of high interest for the XPCS experiments. Presently there is no interest in

pulse lengths below 1 fs in this community. For certain XPCS experiments longer pulses may be of interest.

### **Polarization**

XPCS experiments at larger momentum transfer necessarily desire vertical polarization of the FEL radiation. The angular resolution required to match the speckle size in a wide-angle XPCS experiment can only be achieved with a detector arm of at least 10 m length. Such a long detector arm is only practicable in horizontal scattering geometry. For horizontal polarization in this geometry, however, the scattered intensity drops with increasing momentum transfer and is down to by a factor 4 (as compared to vertical polarization) at 60 degrees detector angle. Since typical wide-angle XPCS experiments will have very low count rates, an additional intensity loss caused by an unsuited polarization should be avoided.

A vertical polarization will also be beneficial for the setup and operation of a reliable variable-energy split and delay line. For vertical polarization an established and robust design on an optical bench can be used.

### **Beamline**

#### **Monochromaticity**

Experiment will either use the natural band width ( $10^{-3}$ ) of the XFEL or use a monochromator. Typically either moderate ( $10^{-4}$ ) or low bandwidth ( $10^{-5}$ ). The latter is the bandwidth of the split and delay line, which can therefore serve as a post monochromator.

#### **Spot size**

Experiments will use a beam size that is compatible with i) an (acceptable) sample heating ii) makes optimum use of the (available) 2D detector system. The spot size should be variable in the range from 200  $\mu\text{m}$  to 1  $\mu\text{m}$  diameter. Certain experiments will use the unfocused beam collimated by variable slits.

#### **Diagnostics**

The XPCS experiments need information about beam intensity, beam position, pulse length and higher harmonic contributions for every pulse. Helpful would further be a diagnostics of the degree of coherence as probed, e.g., by speckle visibility, again on a pulse by pulse basis. This latter probe of course should not destroy the coherence. Depending on how these source parameters vary from pulse to pulse and on other time scales some diagnostics requirements may be relaxed at a later stage.

#### **Detectors**

Three different types of experiments are considered by the XPCS community for the XFEL, which lead to different detector requirements. The detectors that are presently being developed for the XFEL are only usable for XPCS experiments carried out in small-angle scattering geometry or single-shot experiments at larger angles. The community, however, has a high interest in low-count-rate experiments at high scattering angles, for which detectors with a better angular resolution (i.e., smaller pixel size) are required (see III.4 and III.5). The given dimensions of the experimental floor limit the detector arm length in transverse direction, while heat-load and radiation damage thresholds do not allow to increase the speckle size by focusing the beam further if any use of the high repetition rate of the European XFEL should be made. On the other hand for experiments of this kind the required dynamic range is small and radiation-hardness limits can be relaxed. Specifications are summarized in Table 1.

The following types of XPCS experiments are planned:

### Wide-angle dynamics

These are low-count rate experiments at detector angles up to about 60 degrees. The required angular resolution of the detector is 2-3  $\mu\text{rad}$ . In order to achieve this resolution a pixel size well below 100  $\mu\text{m}$  plus a transverse floor space of at least 10 m in the experimental hutch is required. A possible hutch layout is shown in Fig. 13. Because of the low count rates, these experiments can live with a small dynamic range (typically 0 to few events per pixel and frame) of the detector: This should help in reducing the pixel size compared to the presently developed high-dynamic range detectors. In order to obtain a significant counting statistics in an acceptable time  $10^8$  pixels are required. The frame rate should be as high as possible under these specifications.

For experiments of angular correlations, detectors should ideally cover the full diffraction ring of a given momentum transfer range. In order to accommodate such a setup in the experimental hutch a deflection of the photon beam sideways and/or vertically should be planned.

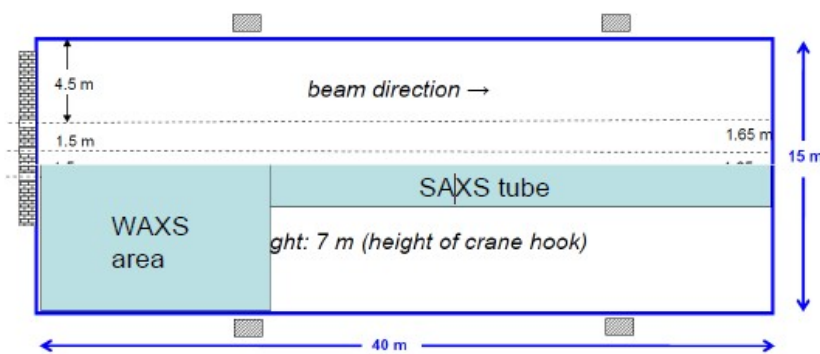


Figure 13:  
Floorplan layout for the MID station.

### Small-angle scattering

The angular resolution of the detector should be 4  $\mu\text{rad}$  (see Table 1). The frame rate should be as high as possible. Countrates  $\leq 100$  / pixel are to be expected.

### Single-shot large Q experiments

These are experiments, which allow damage of the sample by the photon beam by, e.g., rapidly moving the sample across the beam. In this case the beam can be focused to about 1  $\mu\text{m}$  or less on the sample, which in turn relaxes the requirements for the angular resolution of the detector to about 40  $\mu\text{rad}$  or more. This is definitely the case for single shot XCCA experiments at large Q, which require a small sample volume a) for good angular contrast in the 4-point cross correlator function  $C_Q$  and b) because of the limited longitudinal coherence of the x-ray beam. If we are dealing with disordered matter the count rates will still be low so that single photon counting is an option. Not many frames per bunch train need to be stored but some experiments may need a frame rate that matches the XFEL repetition rate. If we are dealing with long-range ordered structures, the requirements are similar to those to be encountered in imaging experiments, where count rates will be high and require a high dynamic range of the detector.

## Sample environment

For XPCS on short time scales a variable energy split and delay line shall be used. Delay times of up to 10 ns are required as well as operation at various energies. For solid samples a diffractometer with cooling and heating stage is required, for liquid samples a setup to study a liquid jet. The sample environment should allow to apply external magnetic fields and pressure. In order to excite the sample a pump laser is requested. The possibility to use THz radiation from the XFEL as a pump source should be explored. Certain studies may involve toxic and or active samples. Provisions to handle such materials should be planned.

A summary of the requirements is given in Table 2.

### Overview of key parameters

|                                |   |
|--------------------------------|---|
| Energy range of first harmonic | 6 – 15 keV  |
| Polarization                   | Vertical  |
| Monochromaticity               | <ul style="list-style-type: none"><li>•<math>10^{-3}</math> (natural band width)</li><li>•<math>10^{-4}</math> with monochromator,</li><li>•<math>10^{-5}</math> with mono and split and delay line</li></ul> |
| Beam spot size                 | <ul style="list-style-type: none"><li>•Variable between 1 <math>\mu\text{m}</math> and 200 <math>\mu\text{m}</math></li><li>•unfocused with slits</li></ul>   |
| Diagnostics: pulse by pulse    | <ul style="list-style-type: none"><li>•Intensity</li><li>•Position</li><li>•Pulse length</li><li>•Higher harmonics content</li><li>•speckle visibility</li></ul>  |
| Detectors                      | Two different types: see Table 1<br>1. SAXS<br>2. WAXS  |
| Hutch, beamline                | <ul style="list-style-type: none"><li>•10 m transversal space</li><li>•40 m longitudinal space</li><li>•provision to deflect the beam sideways and/or upwards</li></ul>                                       |

## V Conclusion

The workshop on the “Materials Imaging and Dynamics Instrument” at the European XFEL confirmed the strategic importance of that instrument for a wide user community. Time domain studies will be a very important discipline at the facility. The workshop has shown that the number of XPCS applications has steadily grown in recent years and important large Q applications (X-ray Cross Correlation Analysis, Atomic Diffusion,..) have been emerging (not discussed in the TDR). The workshop allowed to re-iterate on the requirements, as summarized in Chapter 4. The strategic importance of 2-D detectors has been confirmed and it will be of OUTMOST importance to develop (in close collaboration with the XFEL facility and the detector builders) a strategy that will provide an adapted detector

## VI References

- [1] XFEL: Technical Design Report, 2006, DESY 2006-097
- [2] G. Grübel et al., Nucl. Instr. and Meth. in Phys. Res. B 262 (2007) 357–367
- [3] M. Paulus et al., Phys. Rev. B 78, 235419 (2008)
- [4] J. A. Forrest et al., Phys. Rev. Lett. 77, 2002 (1996)
- [5] C. Gutt et al., Phys. Rev. B79, 212406 (2009)
- [6] C. Gutt et al. , Phys. Rev. B, 81, 100401 (2010)
- [7] P. Wochner et al., PNAS, 106/28, 11511 (2009)
- [8] D.B. Miracle, Nature Materials 3, 697 (2004); H.W. Sheng et al., Nature 439, 419 (2006); D. Ma et al, Nature Materials 8, 30 (2008)
- [9] M. Leitner et al., Nature Materials, 8, 717 (2009)
- [10] L. Cipolletti et al., J. Phys: Condens, Matter 15, S256 (2003); A. Duri et al., Phys. Rev. E 75, 051401 (2006)
- [11] A. Madsen et al., New. J. Phys, 12, 055001 (2010)
- [12] W. Roseker et al., Optics Letters, 34/12, 1768 (2009)

## VII Annex

### VII.1 Participants

|                                 |  |
|---------------------------------|--|
| Massimo Altarelli               | European XFEL, Germany                   |
| Oier Bikondoa                   | XmaS CRG Grenoble, France                |
| Marcel Buchholz                 | University of Cologne, Germany           |
| Chun-Fu Chang                   | University of Cologne, Germany           |
| Marc Boissieu                   | CNRS, Saint-Martin d'Hères, France       |
| Annick Froideval                | PSI, Villingen, Switzerland              |
| Jeroen Goedkoop                 | University of Amsterdam, The Netherlands |
| Heinz Graafsma                  | DESY, Germany                            |
| Gerhard Grübel                  | DESY, Germany                            |
| Christian Gutt                  | DESY, Germany                            |
| Ruslan Kurta                    | DESY, Germany                            |
| Frédéric Livet                  | CNRS, Saint-Martin d'Hères, France       |
| Anders Madsen                   | ESRF, France                             |
| Aymeric Robert                  | LCLS, USA                                |
| Wojciech Roseker                | DESY, Germany                            |
| Christian Schuessler-Langeheine | University of Cologne, Germany           |
| Andreas Schwarz                 | European XFEL, Germany                   |
| Bogdan Sepiol                   | Univ. of Vienna, Austria                 |
| Harald Sinn                     | European XFEL, Germany                   |
| Brian Gregory Stephenson        | Argonne National Laboratory, USA         |
| Masamitsu Takahashi             | Japan Atomic Energy Agency               |
| Peter Wochner                   | Max-Planck Institute Stuttgart, Germany  |
| Mikhail Yurkov                  | DESY, Germany                            |

## VII.2 Estimates of Signal-to-Noise Ratios

The signal to noise ratio is given by  $R_{sn} \propto AI\sqrt{N}$  [1], where A denotes the contrast of the speckle pattern, I the average intensity per pixel and N the number of pixels. XPCS experiments will be limited by beam damage. So the SNR has to be optimized in terms of beamsize W, detector-sample distance R and detector pixel size P.

The speckle size S is given by  $S = \lambda R/W$ .

We write for the intensity per pixel  $I = I_0 P^2 / R^2$  and for the contrast  $A = 1 / (1 + P^2 / S^2)$  (Gaussian approximation). SAXS diffraction patterns are localized in Q-space.

$\Delta\theta$  denotes the angular width of the scattering signal and  $M = (R\Delta\theta)^2$  is the area of scattering on the detector. The number of pixels is therefore  $N = M/P^2$ . We find for

the SNR the expression  $R_{sn} \propto \frac{I_0 \Delta\theta P}{R(1 + P^2 / S^2)}$ , which peaks at  $S=P$ .

Below we plotted some SNR curves.

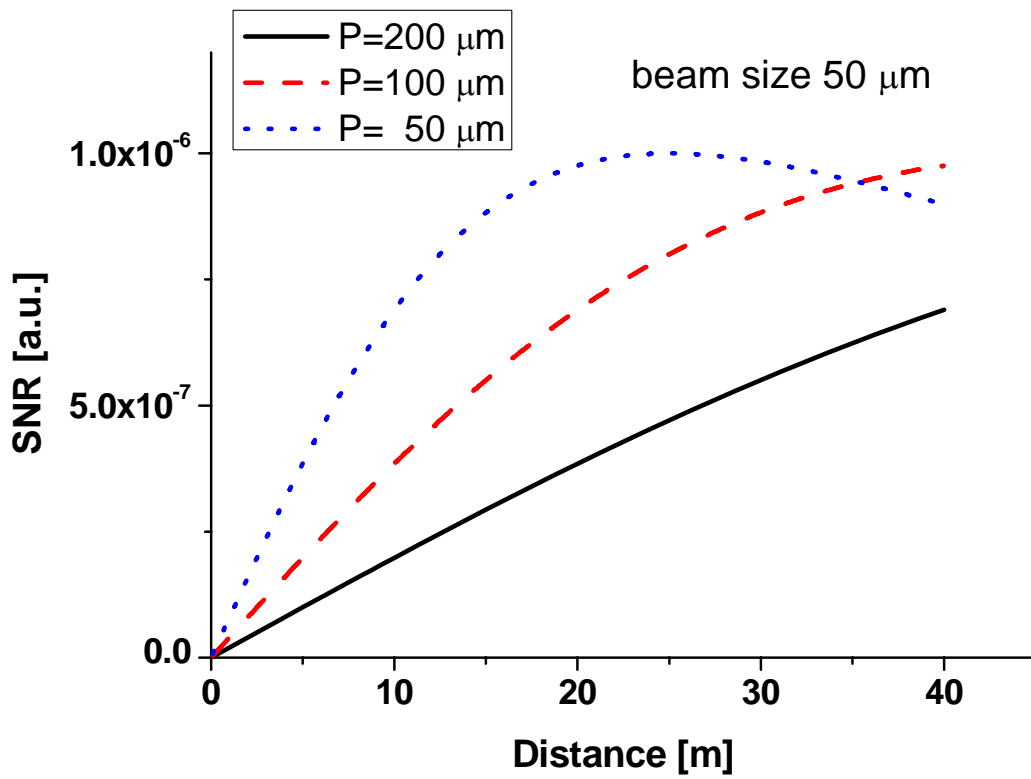
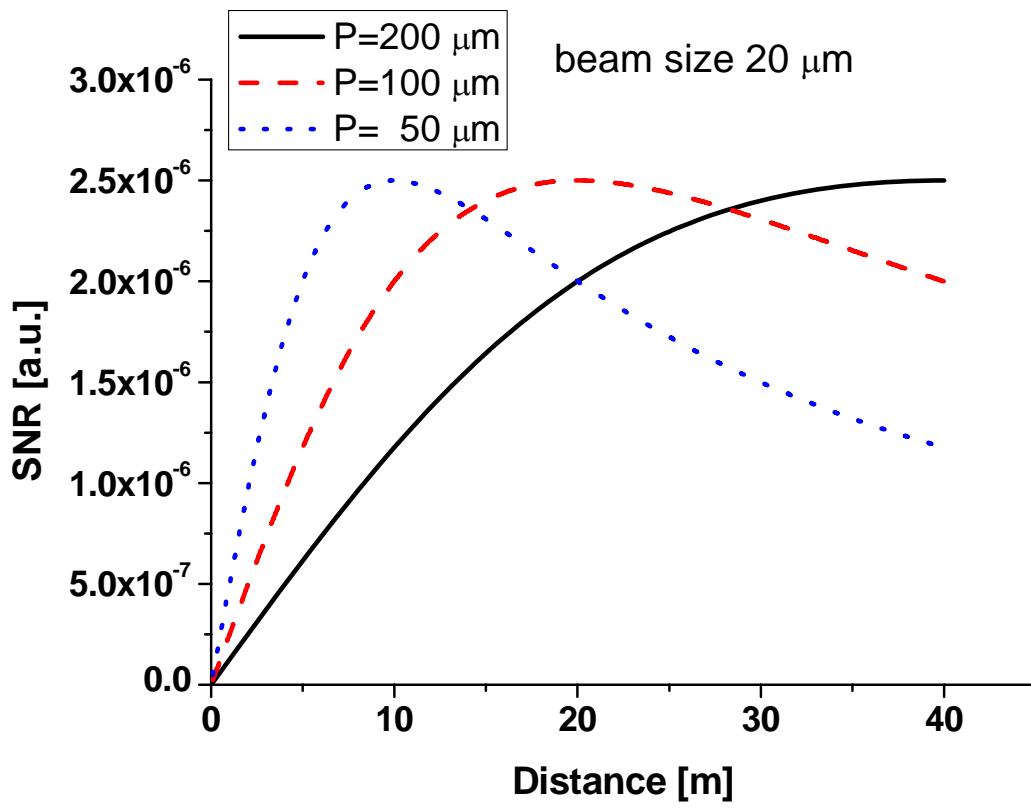
## VII.3 Effect of masking

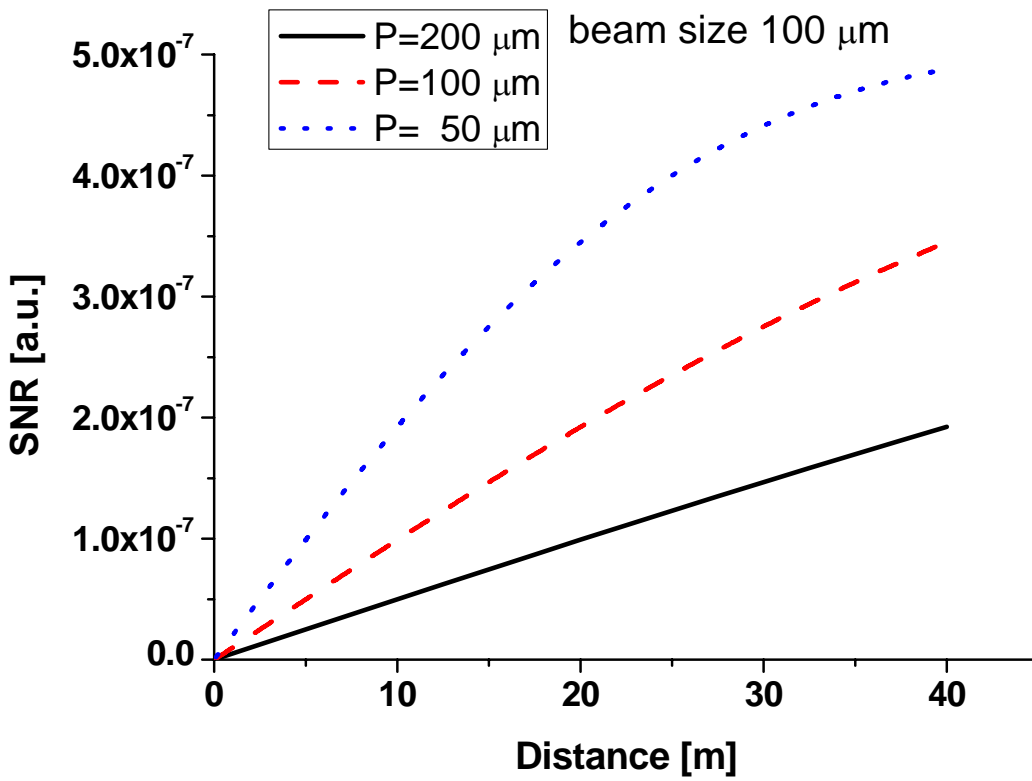
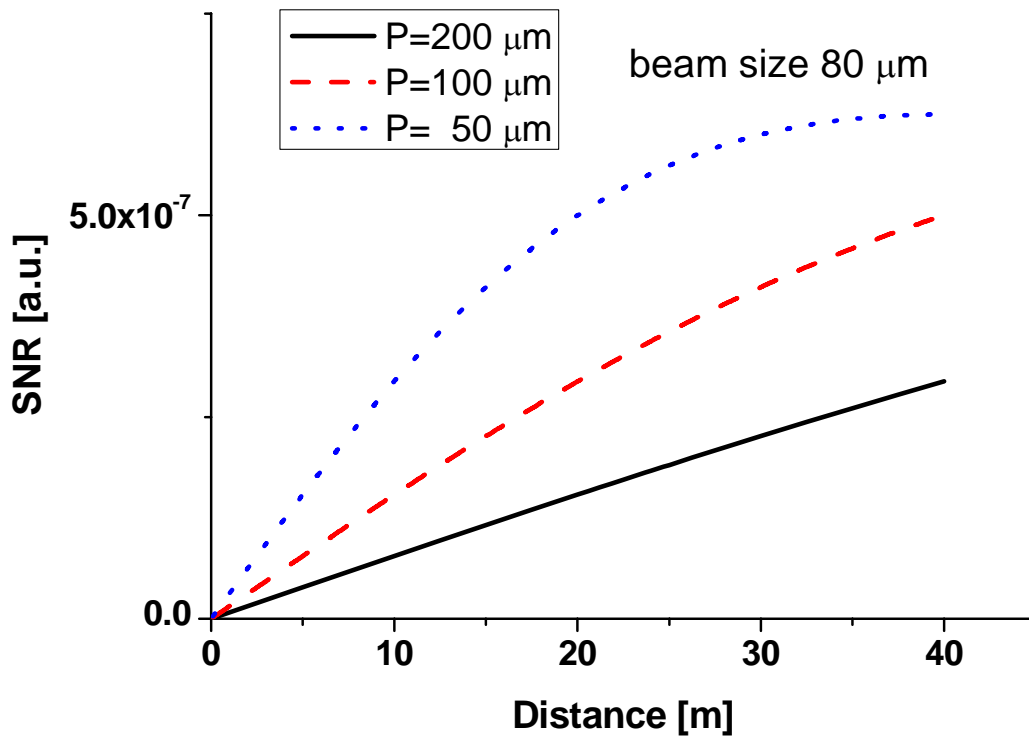
The detector has a pixel size of P. We put a mask on it so the pixel size exposed to the beam is  $P_m$ . We write for the intensity per pixel  $I = I_0 P_m^2 / R^2$  and for the contrast  $A = 1 / (1 + P_m^2 / S^2)$  (Gaussian approximation). As the scattering signal is localized in Q-space and does not cover the whole detector chip the number of pixels is still given

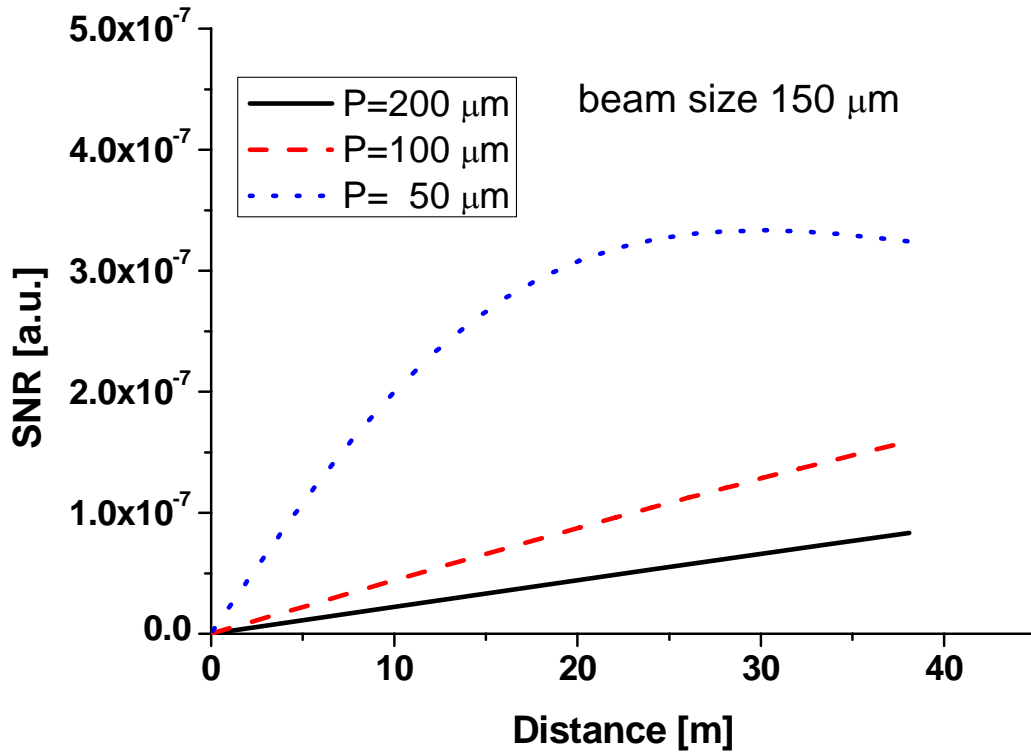
by  $N = M/P^2$ . The SNR is therefore  $R_{mask} \propto \frac{I_0 \Delta\theta P_m^2}{RP(1 + P_m^2 / S^2)}$ . The SNR of a masked and

unmasked detector are shown below for  $P=200$  microns and  $P_m=100$  microns. It can be seen that  $R_{mask} < R_{unmasked}$  for all distances. So masking in forward direction does not help as the increase in speckle contrast is too much penalized by the decrease in intensity per pixel.

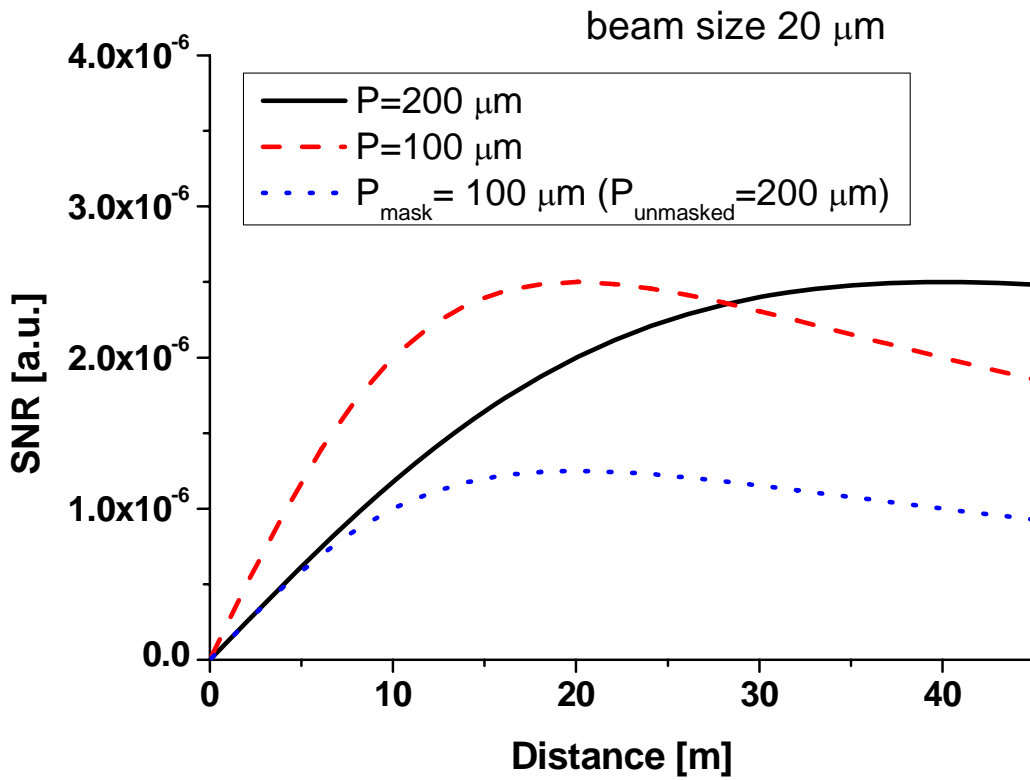
[1] see e.g. P. Falus, L Lurio and S. Mochrie, Journal of Synchrotron Radiation 13, 253 (2006) and references therein







### Masking



## VII.5 Expected properties of the radiation generated by SASE I

Note for participants of MID Instrument Workshop, Grenoble, October 28-29, 2009<sup>1</sup>  
 E.L. Saldin, E.A. Schneidmiller, M.V. Yurkov

Baseline parameters of the electron beam at the European XFEL are: energy 17.6 GeV, peak current 5 kA, bunch charge 1 nC, rms bunch length 24  $\mu\text{m}$ , rms normalized emittance 1.4 mm-mrad, rms energy spread at the linac exit 1 MeV. Parameters of the SASE1 radiator and properties of the radiation at the saturation point are compiled in Table 1. Temporal and spectral properties of the radiation are illustrated with Figs. 1 and 2. Intensity distributions of the radiation field in the near and far zone are shown in Fig. 3.

An important figure of merit for experiments planned at the MID instrument is the degree of transverse coherence. Relevant dependencies are shown in Fig. 4 for different values of the parameter  $\varepsilon^{\wedge} = 2\pi\varepsilon/\lambda$ . General behavior of the degree of transverse coherence is such that it reaches maximum value just before the saturation, and then drops drastically in the nonlinear regime. Such a behavior is defined by poor longitudinal coherence as it has been explained in refs. [2–4].

Special attention should be devoted to the optical transport system to avoid unwilling effects for experiments to be performed at the MID instrument. The first kind of effects relates to the wave front distortions. The second effect originates from a mixing of the longitudinal slices (e.g. in monochromator leading to the degradation of the transverse coherence).

Baseline parameters correspond to the value of  $\varepsilon^{\wedge} = 2.6$  which results in the value for the degree of transverse coherence at the saturation  $\zeta \approx 0.65$ . Here users should clearly realize that there exists a scenario of operation of the European XFEL with parameters deviating significantly from the baseline option. Baseline parameters represent a set of possible beam characteristics which may be obtained at sufficient safety margin of operation of different systems. Most critical parameter is slice emittance which may be significantly less if the beam formation system works perfectly. For instance, such a situation has been realized at LCLS: baseline value for the emittance was 1.2 mm-mrad for the bunch charge of 1 nC while experimentally realized parameter was emittance of about 0.4 mm-mrad at the bunch charge of 0.25 nC. Recent simulation and experimental results for the European XFEL also indicate on the probability of a low-emittance mode of operation. Currently we can discuss realization of the normalized emittance of 0.8 mm-mrad at the bunch charge of 1 nC, and 0.4 mm-mrad at the bunch charge of 0.25 nC. Low-emittance mode of operation is favorable in terms of the degree of transverse coherence: with the normalized emittance of 0.4 we reach the value of  $\varepsilon^{\wedge} \approx 0.8$  which corresponds to the ultimate value for the degree of transverse coherence of about  $\zeta = 0.95$  (see Fig. 5). Another consequences of the low-emittance mode of operation is higher photon pulse energy (inversely proportional to the emittance), and wider angular divergence which should be taken into account when designing optical transport system to the experiment.

<sup>1</sup> This note has been prepared for the participants of the MID Instrument Workshop (Grenoble, October 28-29, 2009). Extended information on the photon beam properties can be also obtained from refs. [1–5].

Table 1  
 Baseline parameters of the SASE1 FEL at the European XFEL [1].

|                          | Units           | Value              |
|--------------------------|-----------------|--------------------|
| Undulator period         | mm              | 35.6               |
| Undulator magnetic field | T               | 1                  |
| Undulator gap            | mm              | 10                 |
| Wavelength range         | nm              | 0.1                |
| Source size (FWHM)       | $\mu\text{m}$   | 70                 |
| Divergence (FWHM)        | $\mu\text{rad}$ | 1                  |
| Bandwidth (FWHM)         | %               | 0.08               |
| Coherence time           | fs              | 0.2                |
| Pulse duration (FWHM)    | fs              | 100                |
| Photons per pulse        | #               | $10^{12}$          |
| Peak brilliance          | B               | $5 \times 10^{33}$ |

### References

- [1] M. Altarelli et al. (Eds.), XFEL: The European X-Ray Free-Electron Laser. Technical Design Report, Preprint DESY 2006-097, DESY, Hamburg, 2006 (see also <http://xfel.desy.de>).
- [2] E.L. Saldin, E.A. Schneidmiller, and M.V. Yurkov, Opt. Commun. 281(2008)1179.
- [3] E.L. Saldin, E.A. Schneidmiller, and M.V. Yurkov, Opt. Commun. 281(2008)4727.
- [4] E.L. Saldin, E.A. Schneidmiller, and M.V. Yurkov, Statistical and coherence properties of radiation from X-ray free electron lasers, submitted to New Journal of Physics.
- [5] G. Geloni, E. Saldin, L. Samoylova, E. Schneidmiller, H. Sinn, Th. Tschentscher, and M. Yurkov, Coherence properties of the European XFEL, submitted to New Journal of Physics.
- [6] E.L. Saldin, E.A. Schneidmiller, and M.V. Yurkov, Nucl. Instrum. and Methods A 429(1999)233.

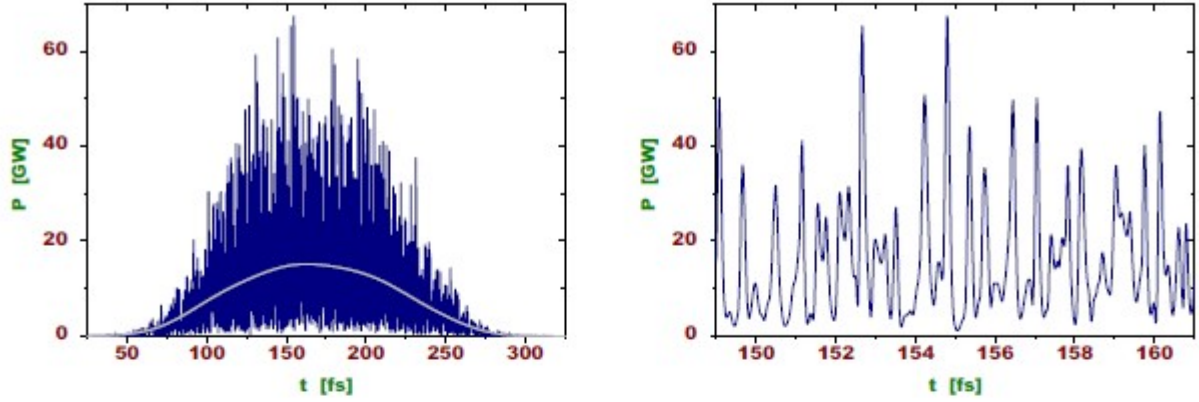


Fig. 1. Temporal structure of the radiation pulse from SASE1. Parameters of SASE1 correspond to baseline parameters (see Table 1). SASE1 operates in the saturation regime. Radiation wavelength is 0.1 nm. Plot at the right-hand side shows enlarged fraction of the plot at the left-hand side. Smooth line shows averaged profile. Calculations have been performed with the simulation code FAST [6].

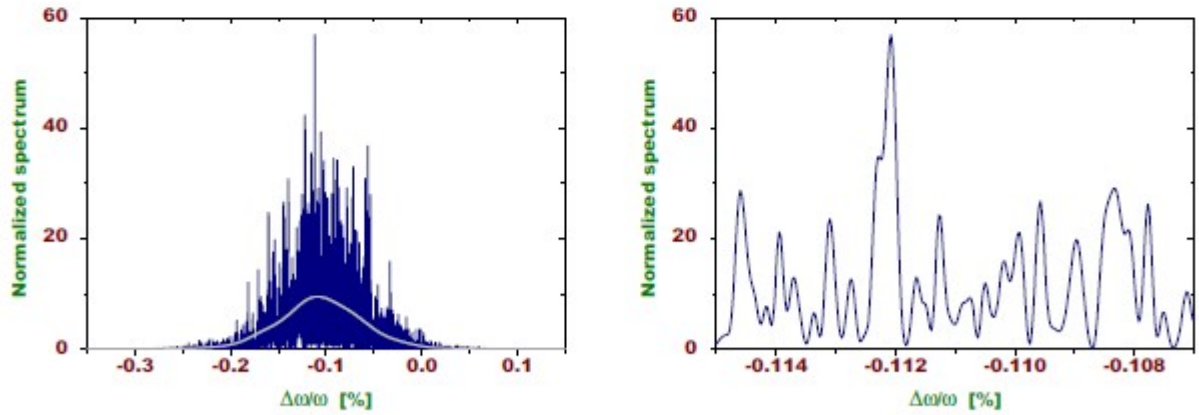


Fig. 2. Spectral structure of the radiation pulse from SASE1. Parameters of SASE1 correspond to baseline parameters (see Table 1). SASE1 operates in the saturation regime. Radiation wavelength is 0.1 nm. Plot at the right-hand side shows enlarged fraction of the plot at the left-hand side. Smooth line shows averaged profile. Calculations have been performed with the simulation code FAST [6].

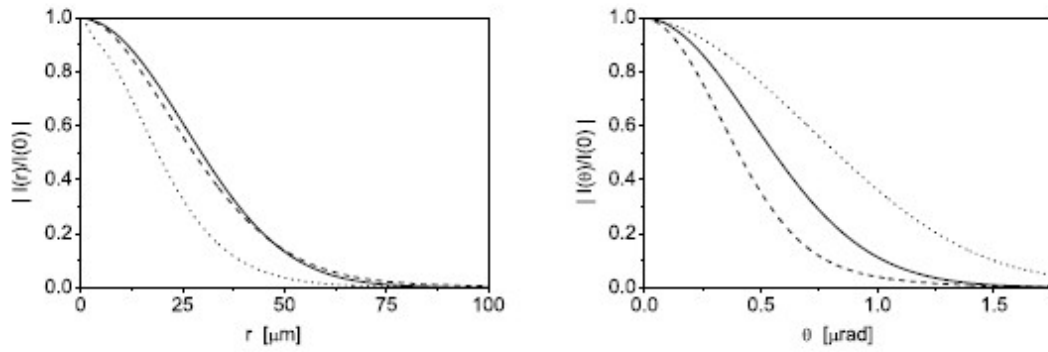


Fig. 3. Intensity distributions of the radiation in the near zone at the undulator exit, and in the far zone (left and right plot, respectively). Parameters of SASE1 correspond to baseline parameters (see Table 1). SASE1 operates in the saturation regime. Radiation wavelength is 0.1 nm. Solid, dotted, and dashed curves correspond to saturation ( $z = z_{\text{sat}}$ ), linear regime ( $z = 0.5z_{\text{sat}}$ ), and deep nonlinear regime ( $z = 1.5z_{\text{sat}}$ ).

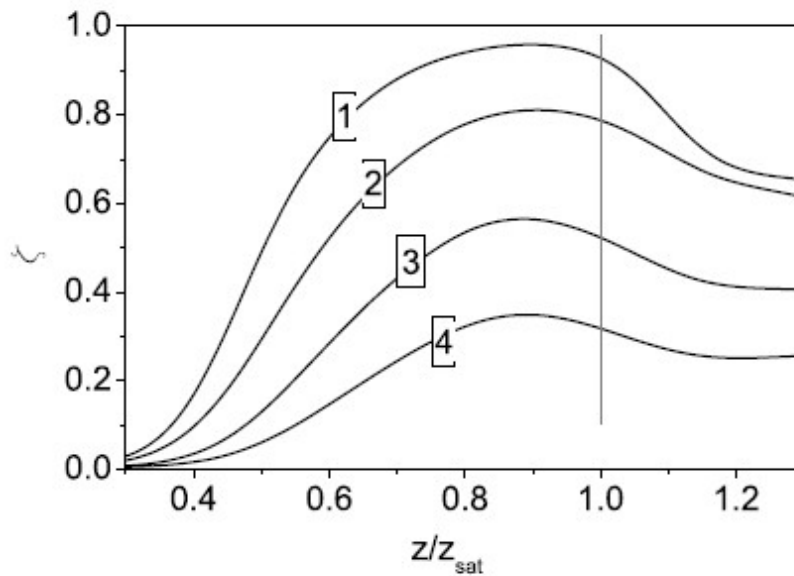


Fig. 4. Evolution of the degree of transverse coherence along the undulator length for  $\hat{\epsilon} = 1, 2, 3,$  and  $4$ . Undulator length is normalized to saturation length. Calculations have been performed with simulation code FAST [6].

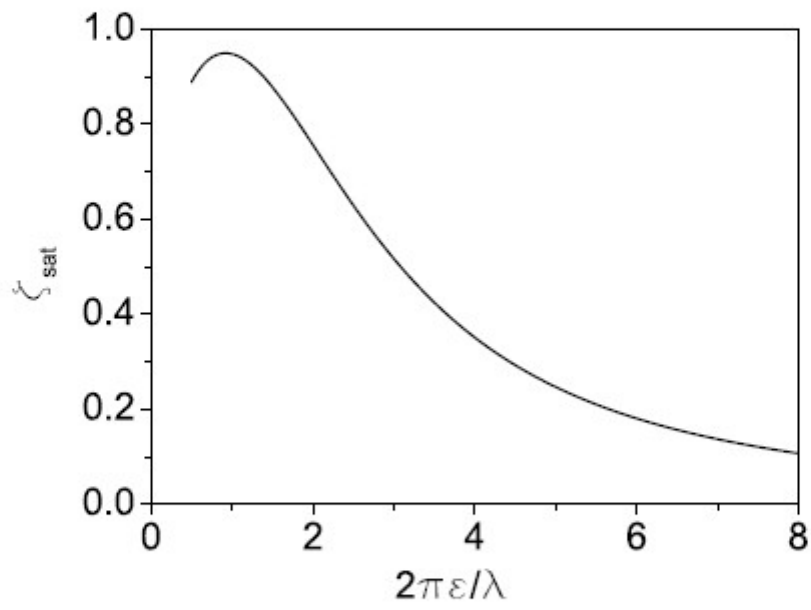


Fig. 5. Degree of transverse coherence  $\zeta_{\text{sat}}$  in the saturation point versus parameter  $\hat{\epsilon}$ . The number of electrons in the coherence volume is  $N_c = 4 \times 10^6$ . Calculations have been performed with the simulation code FAST [6].